Electrooptically-Active Slow-Light-Enhanced Silicon Slot Photonic Crystal Waveguides

Xiaonan Chen, Alan X. Wang, Swapnajit Chakravarty, and Ray T. Chen, *Fellow, IEEE*

***Abstract*—An electrooptically-active 80-nm-slot silicon photonic crystal waveguide is experimentally demonstrated. The index perturbation enhancement of 30 times is demonstrated in a Mach–Zehnder interferometer configuration. The second enhancement factor is the energy confinement within the slot region of the photonic crystal waveguide. The combined effect provides good potential for sensor applications.**

***Index Terms*—Optical-to-electrical detection, sensitivity enhancement, sensor application, slot photonic crystal waveguide.**

I. Introduction

SILICON photonics technology is increasingly important for a myriad of applications [1]–[7]. Silicon-based nanophotonic devices have the advantage of a compact structure with the potential for monolithic integration with optical-to-electrical on-chip conversion and detection [8]. In particular, the slotted waveguide devices recently reported [9], [10] that are able to confine light in a nanoscale low refractive index region are becoming crucial due to the fact that they provide an ideal platform for mode field concentration in the slot region where other materials can be inserted to provide a myriad of new explorations. As another potential solution for sensitivity enhancement in waveguide devices, photonic crystal waveguides (PCWs) are capable of slowing down light to a fraction of its original speed in vacuum by hundreds of times, and hence, greatly improve the interaction with the waveguide material [11]. In this paper, we report defect-engineered PCWs to provide both guided wave confinement and slow light effect that can constitute 60 times of enhancement. PCW offers slow group velocity, and hence, moderately high sensitivity within a continuous spectrum such that the range of the working wavelength extends to 10 nm scale [11], which is two orders of magnitude wider than a microring resonator [9]. We present a universal approach based on phase-shift measurement in order to characterize the sensitivity enhancement of the slot PCW. We also apply plane wave expansion algorithm to simulate the effective index variation of the propagating modes, and hence, justify the approach of device characterization.

Manuscript received January 6, 2009; revised February 5, 2009. Current version published October 7, 2009. This work was supported in part by the Air Force Office of Scientific Research under Grant FA9550-05-C-0171 monitored by Dr. G. Pomrenke, in part by the Defense Advanced Research Projects Agency, in part by the State of Texas, and in part by Sematech.

X. Chen and R. T. Chen are with the Microelectronic Research Center, Department of Electrical and Computer Engineering, The University of Texas, Austin, TX 78758 USA (e-mail: xiaonan_chen@mail.utexas.edu; chen@ece.utexas.edu).

A. Wang and S. Chakravarty are with Omega Optics Inc., Austin, TX 78758 USA (e-mail: alan.wang@omegaoptics.com; swapnajitc@gmail.com).

Color versions of one or more of the figures in this paper are available online at http://ieeexplore.ieee.org.

Digital Object Identifier 10.1109/JSTQE.2009.2016980

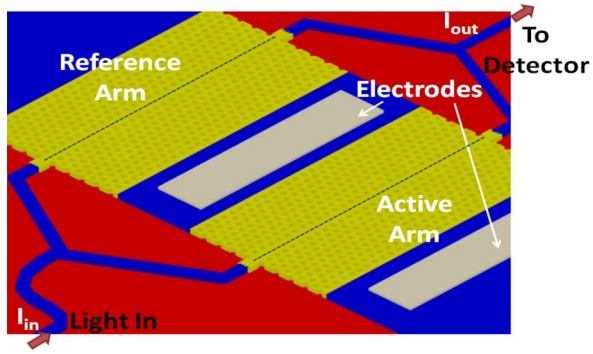

Fig. 1. Schematic diagrams of Mach–Zehnder interferometer with slot PCWs working as the active and reference arms.

II. Waveguide Design and Enhancing Mechanism

A schematic of the dual-enhanced slot PCW structure for phase-shift measurement is depicted in Fig. 1. We integrate the slot PCW in a Mach–Zehnder interferometer in order to measure the phase shift $\Delta\phi$ of the active arm from the output intensity, which is given by

$$I_{\text{out}} = \frac{I_{\text{in}} + I_{\text{in}}\cos(\Delta\varphi)}{2}.$$

One can further derive the effective index change Δn_{eff} of the waveguide mode using the equation

$$\Delta\phi = \frac{2\pi}{\lambda}\Delta n_{\text{eff}} L$$

where L is the active length of the phase shifter, and λ is the wavelength in the free space. The definition of the waveguide sensitivity is given by [3]

$$S = \frac{\Delta n_{\text{eff}}}{\Delta n_c}$$

where Δn_c is the refractive index change of the waveguide material. For convenience, we always characterize the sensitivity enhancement by comparing Δn_{eff} with the same Δn_c profile applied for different waveguide structures.

A cross-section diagram of the active arm is depicted in Fig. 2. The enhancements of the waveguide sensitivity are realized out of the combination of slow light effect and tighter confinement of optical guided wave in the slotted PCW [12]. The refractive index change is generated through free carrier dispersion effect [13], [14], and therefore, is controlled by the carrier concentration profile. We design the silicon slab layer with a uniform doping profile in order to simplify the device fabrication procedure. As shown in Fig. 3, we may control the driving

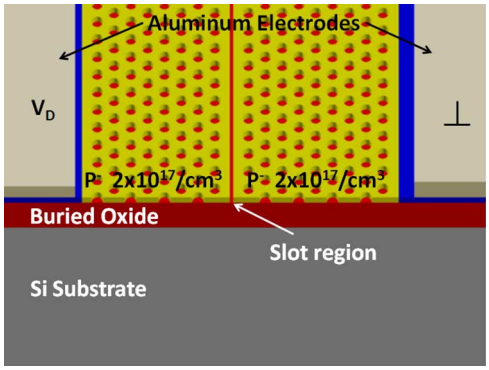

Fig. 2. Cross-sectional view of the slot PCW-based active arm in Mach–Zehnder interferometer.

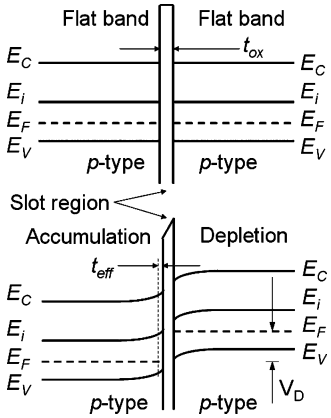

Fig. 3. Energy band diagram of the capacitor-embedded silicon slab layer. The driving voltage V_D switches the left region from flat band to accumulation state.

voltage V_D in order to switch the left silicon region of the lateral capacitor between flat band and accumulation state. When a positive driving voltage is applied to the device, a thin charge layer is accumulated to the left side of the slot while the other side is depleted. The average charge density change ΔN on the left side is related to the driving voltage by [15]

$$V_D = V_{\rm FB} + \frac{q\Delta N t_{\rm ox} t_{\rm eff}}{\varepsilon_{\rm ox}} + \frac{q(\Delta N t_{\rm eff})^2}{2\varepsilon_s N_A}$$

where the flat-band voltage $V_{\rm FB} = 0$ V for a symmetric doping profile, $t_{\rm ox}$ is the slot width, $t_{\rm eff}$ is the effective charge layer width, $\varepsilon_{\rm ox}$ and ε_s are the permittivity of the oxide and silicon regions, respectively, and N_A is the p-type doping concentration of the silicon layer. We can calculate the refractive index change of the accumulation region through an empirical equation [16]

$$\Delta n_c = -8.5 \times 10^{-18} (\Delta N)^{0.8}.$$

A similar model is applied to calculate the refractive index change of the depletion region. The net effect of carrier accumulation and depletion creates the index modulation for the guided mode.

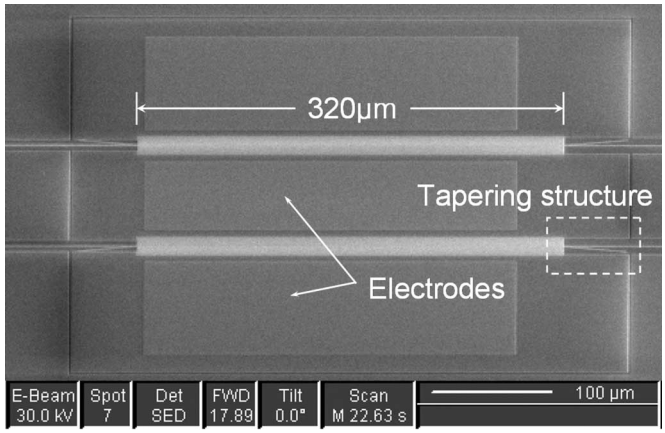

(a)

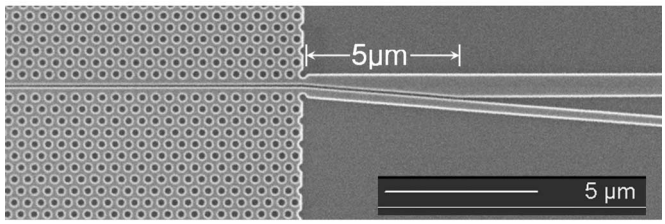

(b)

Fig. 4. (a) Scaning electron microscopy (SEM) top view of the active region integrated with tapering mode couplers. (b) The enlarged tapering structure.

III. Waveguide Fabrication and Performance Evaluation

The capacitor-embedded PCW Mach–Zehnder interferometer shown in Fig. 1 is fabricated on a silicon-on-insulator wafer with p-type background doping at 2×10^{17} cm^3. The thickness of the top silicon layer is 250 nm. We grow a 40 nm thermal oxide layer at 950 °C as a hard mask. Then, we pattern the oxide mask layer using the E-beam lithography technique followed by a standard dry etch pattern transfer. The hexagonal lattice pattern of the slot PCW, which provides the largest band gap among all PCW designs for quasi-2D PCW, is well optimized to provide slow light effect around $\lambda = 1.55$ μm. The lattice constant is 400 nm and the hole diameter is 220 nm. We also employ another thermal oxidation in order to smoothen the surface roughness from the reactive ion etch. Experimental results show that one can reduce the PCW waveguide propagation loss by 2$\sim$3 dB through this procedure. The contact windows for electrodes are opened alongside the slot PCW by a follow-up lift-off process, and the aluminum electrodes are formed afterward. As the last step, the air holes and the center trench are refilled with spin on glass (SOG) followed by 425 °C decarbonization for 1 h. Fig. 4 shows a top view of the resulting device with an air slot. We compose a slotted tapering structure in order to achieve better insulation between both sides of the center oxide trench. A similar tapering structure has been proposed to realize efficient mode coupling between a conventional strip waveguide and a slot waveguide [17]. The propagating mode in the strip waveguide is delocalized by the tapering structure and funneled into the slot PCW through the tilted strip structure.

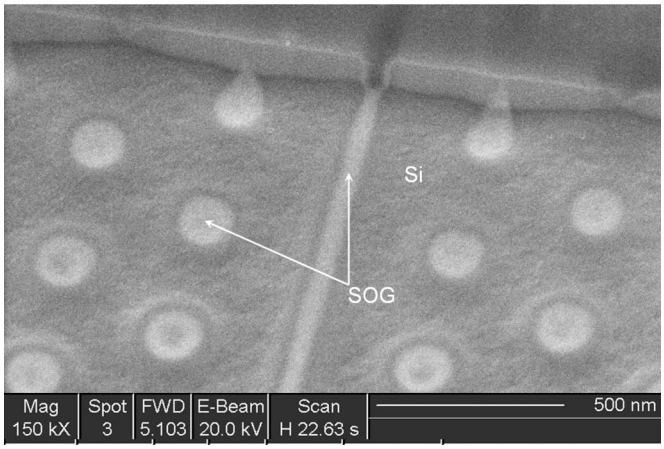

Fig. 5. SEM tilt view of the SOG-filled slot PCW after focused-ion-beam milling.

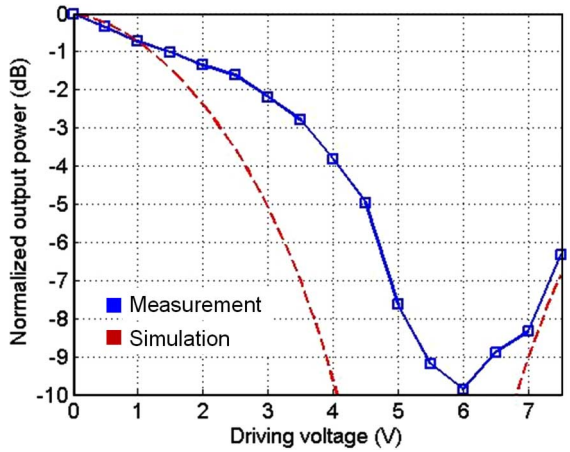

Fig. 6. Optical intensity at the output of the slot PCW-embedded interferometer as a function of the static driving voltage.

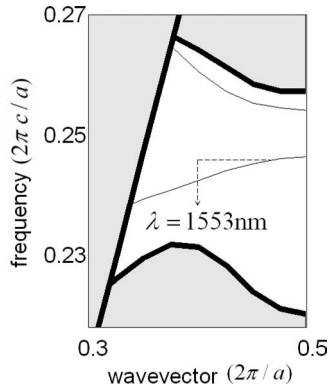

Fig. 7. Band diagram from simulation of the slot photonic crystal waveguide. The thick line is the light line. The gray regions represent the continuum of the extended modes. The thin curves indicate the defect modes.

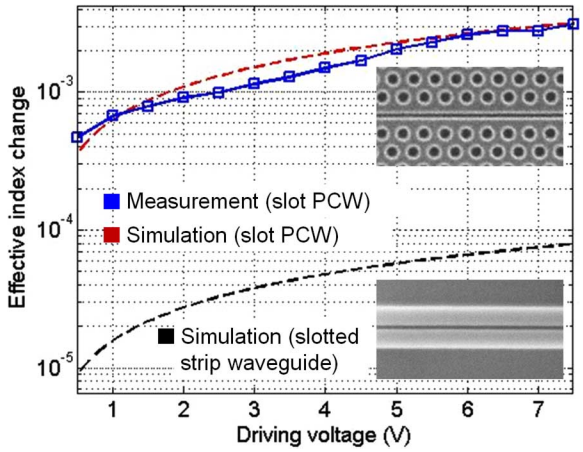

Fig. 8. Comparison of effective index change between a silicon slot PCW and a slotted strip waveguide. The measurement data is derived from the optical intensity curve. The insets show the top-view images of a slot PCW and a slotted strip waveguide, respectively.

A reverse coupling mechanism is applied at the end of the slot PCW. As shown in Fig. 5, we perform a local milling analysis by the focused-ion-beam technique after filling SOG into the air holes and the center narrow trench, and confirm that the holes and the trench have been fully filled with no void formation. The surface is not as smooth as the virgin waveguide due to the roughness induced by the milling process.

We simulate the band diagram of the slot PCW using plane wave expansion algorithm and calculate the variation of the propagation constant as a function of the driving voltage. The optical property of the slot PCW-based Mach–Zehnder interferometer is characterized using a Newport photonics alignment station. Transverse electric polarized at 1553 nm is used for optical measurements. We use polarization-maintaining fibers with lensed taper ends to couple the light into and out of the interferometer device. Fig. 6 shows both measured and simulated optical intensity as a function of the static driving voltage with the corresponding band diagram and the operating point illustrated in Fig. 7. The measurement data show reasonable agreement with the simulation result. The intensity difference at high driving voltage is due to the fact that the mode interference is not perfect at the output junction of the interferometer. The contact resistance also induces a positive V_π shift, which can be minimized through additional heavy doping processes. In order to characterize the sensitivity enhancement of the slot PCW, we perform similar simulation on a slotted strip waveguide and derive the effective index change of the waveguide mode from the optical intensity curve. As indicated in Fig. 8, the slot PCW provides 30 times effective index change compared with the silicon slot waveguide. Our previous finite-difference time-domain simulation [12] shows that the slot PCW confines 48% mode energy within the center narrow slot of 80 nm in width, which indicates a 200% enhancement in energy confinement compared to conventional silicon strip waveguide [18]. Similar confinement effects have also been demonstrated experimentally in both PCW and strip waveguide structures to achieve more efficient control of light propagation [19], [20]. In contrast with slotted strip waveguide, slot PCW slows down the propagation mode, and therefore, provides significant enhancement of light interaction with a moderate reduction of the optical bandwidth.

IV. Conclusion

In conclusion, we present a slot PCW-based interferometer configuration with a universal approach to characterize the sensitivity enhancement compared with silicon slot waveguide. We generate a localized refractive index change through carrier accumulation at the slot boundary. A lateral capacitor model is introduced to simulate the average charge density change as a function of the driving voltage. Both simulation and measurement data demonstrate that the slot PCW exhibits 30-time sensitivity enhancement than the silicon slot waveguide that benefits from the slow light effect at the band edge. Further analysis indicates that such slot PCWs designed with slow light effect have good potential for sensing applications by inserting the active material into the slot.

Acknowledgment

Nanofabrication and characterization facilities used for this work are partially supported by AFOSR, NSF, and NINN.

References

[1] R. G. Heideman, R. P. H. Kooyman, and J. Greve, "Performance of a highly sensitive optical waveguide Mach–Zehnder interferometer immunosensor," *Sens. Actuators B*, vol. 10, no. 3, pp. 209–217, 1993.

[2] B. J. Luff, R. D. Harris, and J. S. Wilkinson, "Integrated-optical directional coupler biosensor," *Opt. Lett.*, vol. 21, no. 8, pp. 618–620, 1996.

[3] H. Sohlström and M. Öberg, "Refractive index measurement using integrated ring resonators," in *Proc. 8th Eur. Conf. Integr. Opt. (EICO '97)*, pp. 322–325.

[4] A. Yalçin, K. C. Popat, J. C. Aldridge, T. A Desai, J. Hryniewicz, N. Chbouki, B. E. Little, O. King, V. Van, S. Chu, D. Gill, M. Anthes-Washburn, M. S. Ünlü, and B. B. Goldberg, "Optical sensing of biomolecules using microring resonators," *IEEE J. Sel. Topics Quantum Electron.*, vol. 12, no. 1, pp. 148–155, Jan./Feb. 2006.

[5] K. De Vos, I. Bartolozzi, E. Schacht, P. Bienstman, and R. Baets, "Silicon-on-insulator microring resonator for sensitive and label-free biosensing," *Opt. Exp.*, vol. 15, no. 12, pp. 7610–7615, 2007.

[6] A. Schweinsberg, S. Hocdé, N. N. Lepeshkin, R. W. Boyd, C. Chase, and J. E. Fajardo, "An environmental sensor based on an integrated optical whispering gallery mode disk resonator," *Sens. Actuators B*, vol. 123, no. 2, pp. 727–732, 2007.

[7] N. A. Mortensen and S. Xiao, "Slow-light enhancement of Beer–Lambert–Bouguer absorption," *Appl. Phys. Lett.*, vol. 90, pp. 141108-1–141108-3, 2007.

[8] B. Jalali and S. Fathpour, "Silicon photonics," *J. Lightw. Technol.*, vol. 24, no. 12, pp. 4600–4615, Dec. 2006.

[9] V. R. Almeida, Q. Xu, C. A. Barrios, and M. Lipson, "Guiding and confining light in void nanostructure," *Opt. Lett.*, vol. 29, no. 11, pp. 1209–1211, 2004.

[10] C. A. Barrios, K. B. Gylfason, B. Sanchez, A. Griol, H. Sohlström, M. Holgado, and R. Casquel, "Slot-waveguide biochemical sensor," *Opt. Lett.*, vol. 32, no. 21, pp. 3080–3082, 2007.

[11] Y. A. Vlasov, M. O' Boyle, H. F. Hamann, and S. J. McNab, "Active control of slow light on a chip with photonic crystal waveguides," *Nature*, vol. 438, pp. 65–69, 2005.

[12] X. Chen, W. Jiang, L. Gu, and R. T. Chen, "20dB-enhanced coupling to slot photonic crystal waveguide using multimode interference coupler," *Appl. Phys. Lett.*, vol. 91, pp. 091111-1–091111-3, 2007.

[13] R. A. Soref and P. J. Lorenzo, "All-silicon active and passive guided-wave components for $\lambda = 1.3$ and 1.6 μm," *IEEE J. Quantum Electron.*, vol. QE-22, no. 6, pp. 873–879, Jun. 1986.

[14] R. A. Soref and B. R. Bennett, "Electrooptical effects in silicon," *IEEE J. Quantum Electron.*, vol. QE-23, no. 1, pp. 123–129, Jan. 1987.

[15] B. G. Streetman and S. Banerjee, *Solid State Electronic Devices*. Upper Saddle River, NJ: Prentice-Hall, 2000, pp. 295–296.

[16] R. A. Soref and B. R. Bennett, "Kramers–Kronig analysis of E-O switching in silicon," *Proc. SPIE*, vol. 704, pp. 32–37, 1986.

[17] J. Blasco and C. A. Barrios, "Compact slot-waveguide/channel-waveguide mode-converter," in *Proc. CLEO Eur.'05*, p. 607.

[18] A. Densmore, D.-X. Xu, P. Waldron, S. Janz, P. Cheben, J. Lapointe, A. Delâge, B. Lamontagne, J. H. Schmid, and E. Post, "A silicon-on-insulator photonic wire based evanescent field sensor," *IEEE Photon. Technol. Lett.*, vol. 18, no. 23, pp. 2520–2522, Dec. 2006.

[19] A. D. Falco, L. O'Faolain, and T. F. Krauss, "Dispersion control and slow light in slotted photonic crystal waveguides," *Appl. Phys. Lett.*, vol. 92, pp. 083501-1–083501-3, 2008.

[20] Q. Xu, V. R. Almeida, R. R. Panepucci, and M. Lipson, "Experimental demonstration of guiding and confining light in nanometer-size low-refractive-index material," *Opt. Lett.*, vol. 29, no. 14, pp. 1626–1628, 2004.

Xiaonan Chen received the B.S. degree in precision instruments and mechanology from Tsinghua University, Beijing, China, and the M.S. degree in electrical and computer engineering from the University of Texas at Austin, Austin.

He is currently working toward the Ph.D. degree at the Microelectronics Research Center, University of Texas at Austin.

Alan X. Wang received the B.S. degree from Tsinghua University, Beijing, China, in 2000 and the M.S. degree in solid-state electronics from the Chinese Academy of Sciences, Beijing, China, in 2003, and the Ph.D. degree in electrical and computer engineering from the University of Texas at Austin, in 2006.

He is currently a Senior Research Scientist at Omega Optics, Austin, TX. His research interests include electrooptic polymer devices, silicon photonic crystal devices, and board level optical interconnects.

Swapnajit Chakravarty received the B.E. degree in electrical engineering from Jadavpur University, Kolkata, India, in 2001, the M.S. degree in electrical engineering from the University of Cincinnati, OH, in 2003, and the Ph.D. degree in electrical engineering from the University of Michigan, Ann Arbor on optically and electrically injected photonic crystal microcavity light emitters, lasers, and chemical sensors.

He is currently a Research Scientist at Omega Optics, Austin, TX.

Ray T. Chen (M'91–SM'98–F'04) received the B.S. degree in physics from National Tsing-Hua University, Hsinchu, Taiwan, in 1980, and the M.S. degree in physics and the Ph.D. degree in electrical engineering from the University of California, San Diego and Irvine, in 1983 and 1988, respectively.

He joined the University of Texas at Austin (UT Austin) as a faculty to start the Optical Interconnect Research Program in the Electrical and Computer Engineering Department in 1992. Prior to his UT's professorship, he was a Research Scientist, Manager, and Director of the Department of Electrooptic Engineering, Physical Optics Corporation, Torrance, CA, from 1988 to 1992. His group at UT Austin has authored or coauthored its research findings in more than 420 published papers including over 55 invited papers. He holds 12 issued patents. His current research interests include three main subjects: 1) nanophotonic passive and active devices for optical interconnect applications; 2) polymer-based guided-wave optical interconnection and packaging; and 3) true time delay (TTD) wideband phased array antenna (PAA).

Prof. Chen is a Fellow of the Optical Society of America and The International Society for Optical Engineers (SPIE). He has served as an Editor or Co-Editor for 18 conference proceedings. He was the recipient of the 1987 UC Regent's Dissertation Fellowship and of the 1999 UT Engineering Foundation Faculty Award for his contributions in research, teaching, and services.